The Astrophysical Journal, 704:915–929, 2009 October 20 doi:10.1088/0004-637X/704/2/915

COMBINING SEMIANALYTIC MODELS WITH SIMULATIONS OF GALAXY CLUSTERS: THE NEED FOR HEATING FROM ACTIVE GALACTIC NUCLEI

C. J. Short and P. A. Thomas
Astronomy Centre, University of Sussex, Falmer, Brighton, BN1 9QH, UK; C.Short@sussex.ac.uk
Received 2009 May 14; accepted 2009 August 18; published 2009 September 25

ABSTRACT

We present hydrodynamical *N*-body simulations of clusters of galaxies with feedback taken from semianalytic models of galaxy formation. The advantage of this technique is that the source of feedback in our simulations is a population of galaxies that closely resembles that found in the real universe. We demonstrate that, to achieve the high entropy levels found in clusters, active galactic nuclei must inject a large fraction of their energy into the intergalactic/intracluster media throughout the growth period of the central black hole. These simulations reinforce the argument of Bower et al., who arrived at the same conclusion on the basis of purely semianalytic reasoning.

Key words: cooling flows – galaxies: clusters: general – hydrodynamics – methods: *N*-body simulations – X-rays: galaxies: clusters

Online-only material: color figures

1. INTRODUCTION

X-ray observations of clusters of galaxies allow us to probe the physical properties of the hot, diffuse intracluster medium (ICM). In the simplest self-similar collapse scenario, where the ICM is heated solely by gravitational processes (such as adiabatic compression and shocks induced by supersonic accretion), we expect the X-ray luminosity L_X of clusters to scale with gas temperature T as $L_X \propto T^2$ (for $T \gtrsim 2$ keV); see Kaiser (1986). However, the observed luminosity–temperature relation is much steeper than predicted, with $L_X \propto T^{2.5-3}$ at $T > 2$ keV (Markevitch 1998; Arnaud & Evrard 1999; Wu et al. 1999; Ettori et al. 2002), becoming steeper still at group scales $T \lesssim 2$ keV (Helsdon & Ponman 2000; Xue & Wu 2000; Osmond & Ponman 2004). This deficit in X-ray luminosity, particularly in low-mass systems, is due to an excess of entropy[1] in cluster cores (Ponman et al. 1999; Lloyd-Davies et al. 2000; Finoguenov et al. 2002). The source of this excess entropy is likely to be a combination of non-gravitational cooling and heating processes (see Voit 2005 for a review).

Radiative cooling leads to an increase in the entropy of the ICM since cold, low-entropy gas condenses to form stars, reducing the gas density and causing higher-entropy gas to flow inward to compensate for the loss of pressure support. This leads to a decrease in X-ray luminosity, breaking the self-similarity of the cluster scaling relations in a way that resembles observations (Bryan 2000; Pearce et al. 2000; Muanwong et al. 2001, 2002; Davé et al. 2002; Voit et al. 2002; Wu & Xue 2002). However, hydrodynamical *N*-body simulations that only include radiative cooling generically predict an excessive amount of cold gas that can form stars (e.g., Suginohara & Ostriker 1998; Lewis et al. 2000; Yoshida et al. 2002); typically the fraction, f_*, of baryons in stars lies in the range 0.3–0.5 in simulated clusters, in clear conflict with the observed value of $f_* \lesssim 0.1$ (Balogh et al. 2001; Lin et al. 2003; Balogh et al. 2008). This highlights the need for extra heating (*feedback*) from astrophysical sources to regulate the cooling flow and quench star formation.

[1] We define entropy as $S = kT/n_e^{\gamma-1}$, where k is Boltzmann's constant, n_e is the electron number density, and $\gamma = 5/3$ is the ratio of specific heats for a monoatomic ideal gas.

Non-gravitational heating, occurring before or during gravitational collapse, raises the entropy of the ICM, preventing gas from reaching high densities in central cluster regions and reducing its X-ray emissivity. This effect will be greater in lower-mass systems, leading to a steepening of the L_X–T relation as desired. The most obvious sources of non-gravitational heating are Type II supernovae (SNe) and active galactic nuclei (AGNs). In the simplest heating models, the energy released by these phenomena is assumed to be injected impulsively into the gas at high redshift. Although not well motivated physically, these so-called *preheating* models have proved capable of reproducing the observed slope and normalization of cluster scaling relations when incorporated in simulations (e.g., Bialek et al. 2001; Brighenti & Mathews 2001; Muanwong et al. 2002; Borgani et al. 2002; Tornatore et al. 2003; Borgani et al. 2005). However, the preheating scenario suffers from several problems. For example, the predicted scatter about the mean L_X–T relation is much smaller than observed and large isentropic cores are generated in low-mass systems that are not seen (e.g., Ponman et al. 2003; Pratt et al. 2006).

Recently, attention has shifted to more realistic models which attempt to couple cooling, star formation and black hole growth with feedback from SNe and AGNs. There has been considerable effort to include such processes in hydrodynamical simulations of galaxy groups and clusters. However, an explicit treatment is unfeasible since star formation, black hole growth, and associated feedback all occur on scales much smaller than can be resolved with present computational resources. The only option is to develop phenomenological prescriptions and assess their validity by comparing the properties of simulated clusters with as much observational data as possible.

Various theoretical models of stellar feedback have been proposed and can be grouped in two basic categories: *thermal*, where the available supernova energy is used to raise the temperature of neighboring gas particles, and *kinetic*, where neighboring particles are given a velocity "kick." Cosmological simulations with radiative cooling, star formation, and supernova feedback yield ICM profiles and scaling relations that are in reasonable agreement with observations, for both thermal (e.g., Valdarnini 2003; Kay 2004; Kay et al. 2004, 2007; Nagai et al. 2007) and kinetic (e.g., Borgani et al. 2004, 2005;

Romeo et al. 2006) models. In particular, the mean L_X–T relation is generally well reproduced on cluster scales $T \gtrsim 2$ keV. However, X-ray luminosities are found to be substantially larger than the observed values on group scales. Other problems are that observed baryon fractions are typically smaller than in simulations (e.g., Kravtsov et al. 2005; Ettori et al. 2006), and star formation is still too efficient, indicating that additional feedback mechanisms are required to offset radiative cooling.

The favored candidate is the gravitational energy liberated by the accretion of gas onto central supermassive black holes within galaxies. This can be extremely large, of the order $10^{62}(M_{\rm BH}/10^9\,M_\odot)$ erg, where $M_{\rm BH}$ is the black hole mass. Analytical calculations suggest that the L_X–T relation of groups can be accounted for if $\sim$1% of the energy released by AGNs is coupled to the surrounding ICM (e.g., Cavaliere et al. 2002). The precise details of how this energy is transferred to the ICM are not well understood at present, but it appears that there are two major channels via which black holes interact with their surroundings (see McNamara & Nulsen 2007 for a review).

At high redshift, mergers of gas-rich galaxies occur frequently and are expected to funnel copious amounts of cold gas toward galactic centers, leading to high black hole accretion rates and radiating enough energy to support the luminosities of powerful quasars. Quasar-induced outflows have been observationally confirmed in a number of cases (e.g., Chartas et al. 2003; Crenshaw et al. 2003; Pounds et al. 2003), and demonstrated in high-resolution simulations of galaxy mergers. In such simulations, it is usually assumed that a small fraction of the bolometric luminosity can couple thermally to the surrounding gas. This approach has been shown to successfully reproduce the observed black hole–bulge mass relation (Di Matteo et al. 2005; Robertson et al. 2006a) and explain the red colors (Springel et al. 2005a), X-ray haloes (Cox et al. 2006), and fundamental plane relation (Robertson et al. 2006b) of massive elliptical galaxies. Di Matteo et al. (2008) recently extended this work to fully cosmological simulations, obtaining similarly encouraging results.

There is another mode of AGN feedback which is not related to quasar activity or triggered by galaxy mergers. Evidence for this can be seen, for example, in brightest cluster galaxies (BCGs) which contain X-ray cavities filled with relativistic plasma (e.g., Blanton et al. 2001; Bîrzan et al. 2004; McNamara et al. 2005; Fabian et al. 2006). These radio-loud X-ray depressions, referred to as *bubbles*, are thought to be inflated by relativistic jets launched from the central black hole. Bubbles may rise buoyantly, removing some of the central cool gas and allowing it to mix with hotter gas in the outer regions of groups and clusters. Together with the accompanying mechanical heating, this can constitute an efficient mechanism for suppressing cooling flows. Simulations of idealized clusters, performed with hydrodynamical mesh codes, suggest that this is indeed the case (e.g., Churazov et al. 2001; Quilis et al. 2001; Ruszkowski & Begelman 2002; Brüggen et al. 2002; Brüggen 2003; Dalla Vecchia et al. 2004).

The first attempt to implement a self-consistent model of black hole growth and heating by AGN-driven bubbles in cosmological simulations was made by Sijacki & Springel (2006). They found that bubble injection can substantially affect the properties of the ICM, especially in massive, relaxed systems at late times. In particular, bubbles are able to efficiently heat central cluster gas, reducing the amount of cold baryons and star formation in the central cD galaxy. Furthermore, the gas density is reduced and the temperature is increased out to radii $\sim$300 h^{-1} kpc, leading to a decline in X-ray luminosity and establishing a flat entropy profile in central regions. Such trends are precisely what is required to reconcile simulations of galaxy clusters with observations.

Following this work, Sijacki et al. (2007) have formulated a unified model of AGN feedback, incorporating both "quasar" and "radio" modes, as well as star formation and feedback from SNe. Motivated by the properties of X-ray binaries (e.g., Fender et al. 1999; Gallo et al. 2003), the transition between the two states is assumed to be governed by an accretion rate threshold $\chi_{\rm radio} = \dot{M}_{\rm BH}/\dot{M}_{\rm Edd}$, where $\dot{M}_{\rm Edd}$ is the Eddington accretion rate. Quasar-like feedback occurs for accretion rates greater than $\chi_{\rm radio}$, while mechanical bubble heating takes place otherwise. This model has recently been used by Puchwein et al. (2008) to investigate the L_X–T relation and gas fractions of galaxy groups and clusters in cosmological simulations. They demonstrated that AGN feedback reduces the X-ray luminosities of groups and poor clusters more than rich clusters, resulting in a steepening of the L_X–T relation on group scales. In fact, the X-ray properties of their simulated objects are in excellent agreement with observational data on all mass scales. However, since their sample size is quite small (21 objects), it is unclear whether their model can generate a realistic population of cool core (CC) and non-cool core (NCC) systems and thus explain the observed scatter about the mean L_X–T relation. The gas fraction in groups and poor clusters was shown to decrease significantly with the inclusion of AGN heating (even though fewer baryons were converted into stars), because gas is driven from central regions to cluster outskirts. In more massive systems, the main effect of AGN feedback is to lower the central gas density and substantially reduce the number of stars formed. However, even with stellar and AGN feedback, the stellar fraction within the virial radii of their simulated objects appears larger than observations suggest, implying that the cooling flow problem has not been fully resolved.

In this paper, we pursue a different, but complementary, approach to the theoretical study of groups and clusters of galaxies. Instead of undertaking fully self-consistent hydrodynamical simulations, we investigate what current semianalytic models (SAMs) of galaxy formation predict for the thermodynamical properties of the ICM. Our goal is to extend the predictive power of these models, thus providing additional constraints on, and insights into, the physics of galaxy formation. We hope that our work will be useful for guiding the development of future SAMs that can simultaneously account for the properties of both the galaxy distribution and the ICM.

The basis of a SAM is a set of dark matter halo merger trees, usually obtained from a high-resolution N-body simulation. The behavior of baryonic matter within these dark haloes is modeled using analytical "recipes" to capture the essential physical processes involved in the formation and evolution of galaxies: gas cooling, star formation, black hole growth, feedback, galaxy dynamics, galaxy mergers, etc. These recipes typically contain a number of adjustable parameters, which are tuned to attain the best possible match to selected observational properties of the galaxy distribution. This semianalytic approach has proved largely successful, reproducing many key properties of real galaxies such as luminosities, colors, star formation rates, the Tully–Fisher relation and the black hole–bulge mass relation (e.g., Kauffmann et al. 1999; Cole et al. 2000; Kauffmann & Haehnelt 2000; Benson et al. 2003; De Lucia et al. 2004; Granato et al. 2004; Bower et al. 2006; Croton et al. 2006; Cattaneo et al. 2006; Menci et al. 2006; Monaco et al. 2007; Font et al. 2008).

The essence of our method is to generate a semianalytic galaxy catalog for a cosmological *N*-body simulation, compute the energy released by SNe and the AGN in each model galaxy, and inject this energy at the appropriate position and time into the baryonic component of a non-radiative hydrodynamical simulation that has the *same* distribution of dissipationless dark matter. In this way, we can track the effect of energy feedback from semianalytic galaxies on the intracluster gas. A similar technique has already been used to study the metal enrichment of the ICM (Cora 2006; Cora et al. 2008).

There are several benefits of our hybrid approach. First, feedback is guaranteed to originate from a galaxy population whose observational properties agree well with those of real galaxies. This is generally not the case in self-consistent hydrodynamical simulations. Second, we only need a single dark matter simulation to construct a semianalytic galaxy catalog. Since *N*-body simulations are much less computationally demanding than hydrodynamical simulations, we can, in principle, attain significantly greater resolution for the collisionless component. With a high-resolution dark matter simulation we can construct a comprehensive galaxy catalog and thus a detailed model for feedback from galaxies. Third, the energy transferred to the ICM by SNe and AGNs can be calculated directly from the semianalytic galaxy catalog, before coupling the SAM to a hydrodynamical simulation. By avoiding the need to include an explicit sub-grid model for star formation, black hole growth, and associated feedback processes, the hydrodynamical simulations we use to track the injection of energy into the ICM require considerably less computational effort. Finally, as we shall see, a lower resolution can be used for the gas than the dark matter in our hydrodynamical simulations. As a result, our technique is readily applicable to large cosmological volumes, allowing massive clusters to be simulated.

The layout of this paper is as follows. In Section 2, we discuss our numerical method in detail, describing the simulations used, the relevant components of the SAM and our feedback implementation. We use our hybrid approach to investigate the bulk properties of the ICM in Section 3, comparing our results with a selection of observational data. A resolution test is presented in Section 4 to demonstrate the robustness of our results. We summarise our results and conclude in Section 5.

2. THE NUMERICAL MODEL

Our hybrid technique for studying the effect of galaxy feedback on intracluster gas consists of three distinct components: an underlying dark matter simulation, a semianalytic galaxy catalog built on the halo merger trees of this simulation, and a hydrodynamical simulation to track the energy injection from model galaxies. In this section, we provide a detailed description of each part of the modeling process.

2.1. Dark Matter Simulations

The cosmological model we adopt is a spatially flat ΛCDM model with cosmological parameters $\Omega_{\rm m,0} = 0.25$, $\Omega_{\Lambda,0} = 0.75$, $h = 0.73$, $n_{\rm s} = 1$, and $\sigma_{8,0} = 0.9$. Here, $\Omega_{\rm m,0}$ and $\Omega_{\Lambda,0}$ are the total matter and dark energy density parameters, h is the Hubble parameter H_0 in units of 100 km s^{-1} Mpc^{-1}, $n_{\rm s}$ is the spectral index of primordial density perturbations, and $\sigma_{8,0}$ is the rms linear density fluctuation within a sphere of radius $8\ h^{-1}$ Mpc. The subscript 0 signifies the value of a quantity at the present day. While there is some tension between our chosen parameter values (particularly $n_{\rm s}$ and $\sigma_{8,0}$) and those derived from the five-year *Wilkinson Microwave Anisotropy Probe* (*WMAP*) data (Dunkley et al. 2009), we have deliberately used the same cosmological parameters as the Millennium simulation (Springel et al. 2005b) since we eventually hope to apply our technique to the full Millennium volume, using the publicly available Millennium semianalytic galaxy catalogs (Lemson 2006) as input.

Initial conditions were created at a redshift $z_{\rm i} = 127$ by displacing particles from a glass-like distribution, so as to form a random realisation of a density field with a ΛCDM linear power spectrum obtained from CMBFAST (Seljak & Zaldarriaga 1996). The amplitudes and phases of the initial density perturbations were chosen to be the same as those of the Millennium simulation initial conditions. We generated initial conditions for two cubic simulation volumes: one with a comoving side length $L = 62.5\,h^{-1}$ Mpc and $N_{\rm DM} = 270^3$ dark matter particles, and the other with $L = 125\,h^{-1}$ Mpc and $N_{\rm DM} = 540^3$. The mass of a dark matter particle is then $m_{\rm DM} = 8.61 \times 10^8\,h^{-1}\,M_\odot$, as in the Millennium simulation. The smaller of these simulations is for the purposes of initial model discrimination, while the larger simulation is to demonstrate our best model in a more cosmologically interesting volume.

The massively parallel tree *N*-body/SPH code GADGET-2 (Springel 2005) was then used to evolve the initial conditions to $z = 0$, with full particle data stored at the 64 output redshifts of the Millennium simulation: $z_{63} = 127$, $z_{62} = 80$, $z_{61} = 50$, $z_{60} = 30$ and $\log_{10}(1 + z_n) = n(n + 35)/4200$, $0 \leqslant n < 60$. The Plummer-equivalent gravitational softening length was fixed at $\epsilon = 40\ h^{-1}$ kpc in comoving coordinates until $z = 3$, then fixed in physical coordinates thereafter. Note that gravitational forces were softened on a fixed comoving scale of $\epsilon = 5\ h^{-1}$ kpc in the Millennium simulation, a factor of 2 smaller than our $z = 0$ softening length. We chose a larger softening scale for two reasons. First, by comparing the number of dark matter substructures (see below) formed in simulations with $\epsilon = 5\ h^{-1}$ kpc and $\epsilon = 10\ h^{-1}$ kpc, we found that the more aggressive softening scheme yields fewer low-mass objects because of two-body heating effects. This means that we can construct a more detailed semianalytic galaxy catalog by setting $\epsilon = 10\ h^{-1}$ kpc. Second, we will be incorporating gas particles into our dark matter simulations and it has been shown that an optimal choice for the softening length in hydrodynamical simulations is approximately 4% of the mean interparticle spacing, corresponding to $\epsilon \approx 10\ h^{-1}$ kpc in our case (Thomas & Couchman 1992; Borgani et al. 2006).

2.1.1. Dark Matter Haloes, Substructure, and Merger Tree Construction

Dark matter haloes are identified as virialised particle groups within the simulations using the friends-of-friends (FOF) algorithm. We adopt a standard FOF linking length of 20% of the mean particle separation (Davis et al. 1985) and only save groups that contain at least 20 particles, so that the minimum halo mass is $1.7 \times 10^{10}\ h^{-1}\ M_\odot$. FOF group catalogs are produced on the fly and in parallel by the simulation code. An improved version of the SUBFIND algorithm (Springel et al. 2001) is then applied in post-processing to these group catalogs to find gravitationally bound dark matter substructures orbiting within the FOF haloes.

To compute a virial mass estimate for each FOF halo, a sphere is grown about the minimum of the gravitational potential within the group until the mean overdensity

enclosed reaches $\Delta\rho_{\rm cr}(z)$, where Δ is the desired density contrast, $\rho_{\rm cr}(z) = 3H_0^2E(z)^2/8\pi G$ is the critical density and $E(z)^2 = \Omega_{\rm m,0}(1+z)^3 + \Omega_{\Lambda,0}$ in a ΛCDM cosmological model. The mass enclosed within the sphere, M_Δ, is then related to the sphere radius, r_Δ, and the circular velocity, v_Δ, at this radius by

$$M_\Delta = \frac{4\pi}{3} r_\Delta^3 \Delta\rho_{\rm cr}(z) = \left[\frac{3}{4\pi G^3 \Delta\rho_{\rm cr}(z)}\right]^{1/2} v_\Delta^3. \quad (1)$$

Following Croton et al. (2006), a density contrast $\Delta = 200$ is used to define the virial mass, radius and velocity of a halo throughout this paper.

Once all haloes and subhaloes have been identified for each simulation output, we construct *merger trees* that describe how haloes grow as the universe evolves. This is done by exploiting the fact that each halo will have a unique descendant in a hierarchical scenario of structure formation; see Springel et al. (2005b) for further details. Each individual merger tree then contains the full formation history of a given halo at $z = 0$.

2.2. The Semianalytic Model of Galaxy Formation

Dark matter halo merger trees form the backbone of modern hierarchical models of galaxy formation. We have generated galaxy catalogs for our two dark matter simulations by applying a SAM to the merger trees. The SAM we use is the highly successful Munich L-Galaxies model described by De Lucia & Blaizot (2007). We adopt the same set of model parameters as De Lucia & Blaizot (2007) since these parameters were used to produce the publicly available Millennium galaxy catalog. As in the full Millennium catalog, galaxy and host halo properties are stored at the same 64 redshift values as the simulation outputs. We now review the components of this model that are relevant for our work; for a full description of L-Galaxies, we refer the reader to Croton et al. (2006) and De Lucia & Blaizot (2007).

2.2.1. Star Formation and Supernova Feedback

The infall of gas into the potential well of a dark halo causes the gas to be shock heated to the halo virial temperature. At late times and in massive systems, this gas is added to a quasi-static hot atmosphere that extends roughly to the virial radius of the dark halo. Gas from the inner regions of this atmosphere can then cool and accrete onto a central cold gas disk. At early times and in lower mass systems, the post-shock cooling time is sufficiently short that a quasi-static halo cannot form. Instead the shocked gas rapidly cools and settles onto the cold disk.

Once gas in the cold disk exceeds a critical surface density, it can collapse and form stars (Kennicutt 1989). Massive stars rapidly complete their life cycle and explode as Type II SNe, injecting gas, metals, and energy into the surrounding medium, reheating cold disk gas and possibly ejecting gas from the quasi-static hot halo. For a given mass Δm_* of stars formed over some finite time interval, the amount of energy released by Type II SNe that is available for heating gas is approximated by

$$\Delta E_{\rm SN} = \frac{1}{2}\epsilon_{\rm halo}\Delta m_* v_{\rm SN}^2, \quad (2)$$

where $v_{\rm SN} = 630$ km s^{-1}, based on a standard stellar initial mass function (IMF), and $\epsilon_{\rm halo}$ is an efficiency parameter. The published value for this parameter is $\epsilon_{\rm halo} = 0.35$ (Croton et al. 2006). We note that the mass actually locked-up in stars is given by $\Delta M_* = (1-R)\Delta m_*$, the rest is assumed to be instantaneously returned to the cold disk. Here R is the recycle fraction, which is assigned the value $R = 0.43$ in accordance with the Chabrier IMF (Chabrier 2003) employed by De Lucia & Blaizot (2007).

The mass of cold gas reheated by SNe is modeled as

$$\Delta m_{\rm reheated} = \epsilon_{\rm disk}\Delta m_*, \quad (3)$$

where $\epsilon_{\rm disk}$ is a parameter that is set to $\epsilon_{\rm disk} = 3.5$, motivated by the observational work of Martin (1999). If the reheated gas were added to the hot halo without changing its specific energy, its total thermal energy would increase by

$$\Delta E_{\rm hot} = \frac{1}{2}\Delta m_{\rm reheated} v_{\rm vir}^2. \quad (4)$$

If there is any excess energy after reheating, i.e., $\Delta E_{\rm SN} > \Delta E_{\rm hot}$, then it is assumed that a mass

$$\Delta m_{\rm ejected} = \left[\epsilon_{\rm halo}\left(\frac{v_{\rm SN}}{v_{\rm vir}}\right)^2 - \epsilon_{\rm disk}\right]\Delta m_* \quad (5)$$

of hot gas is ejected from the halo into an external "reservoir." When $\Delta E_{\rm SN} < \Delta E_{\rm hot}$, there is insufficient energy to eject any gas out of the halo and $\Delta m_{\rm ejected}$ is set to zero. Note that the reheated mass is not reduced in this case. It follows from Equation (5) that no hot gas can be expelled if $v_{\rm vir} > (\epsilon_{\rm halo}/\epsilon_{\rm disk})^{1/2} v_{\rm SN} \approx 200$ km s^{-1}, whereas the entire hot halo can be ejected for small $v_{\rm vir}$.

2.2.2. Black Hole Growth and Cooling Flow Suppression

The growth of supermassive black holes in L-Galaxies is driven primarily by quasar mode accretion, as a result of galaxy mergers. Black holes can grow either by merging with each other or by the accretion of cold disk gas. The coalescence of black holes is modeled simply by taking the sum of the progenitor black hole masses. The gas mass $\Delta M_{\rm BH,Q}$ accreted during a merger of galaxies with respective masses $M_{\rm sat}$ and $M_{\rm central}$ is

$$\Delta M_{\rm BH,Q} = \frac{f_{\rm BH}(M_{\rm sat}/M_{\rm central})M_{\rm cold}}{1 + (280\ {\rm km\ s^{-1}}/v_{\rm vir})^2}, \quad (6)$$

where $M_{\rm cold}$ is the total cold gas mass present and the constant $f_{\rm BH} = 0.03$ is chosen to reproduce the observed local black hole–bulge mass relation. Black hole accretion occurs during both minor ($M_{\rm sat} \ll M_{\rm central}$) and major ($M_{\rm sat} \approx M_{\rm central}$) mergers, although the efficiency in the former case is reduced by the $M_{\rm sat}/M_{\rm central}$ term.

Once a static hot halo has formed around the host galaxy of a black hole, it is assumed that there is also continual and quiescent accretion onto the central black hole directly from the hot phase. The growth rate $\dot{M}_{\rm BH,R}$ of the black hole in this radio mode is described by

$$\dot{M}_{\rm BH,R} = \kappa_{\rm AGN}\left(\frac{M_{\rm BH}}{10^8\ M_\odot}\right)\left(\frac{f_{\rm hot}}{0.1}\right)\left(\frac{v_{\rm vir}}{200\ {\rm km\ s^{-1}}}\right)^3, \quad (7)$$

where $f_{\rm hot}$ is the fraction of the total halo mass in the form of hot gas and $\kappa_{\rm AGN}$ is a free parameter controlling the efficiency of accretion. A value of $\kappa_{\rm AGN} = 7.5 \times 10^{-6}\ M_\odot$ yr^{-1} is found to reproduce the turnover at the bright end of the galaxy luminosity function (De Lucia & Blaizot 2007). This simple phenomenological model may represent the accretion of cold gas clouds, or Bondi–Hoyle accretion from hot gas that fills the space between these clouds (Croton et al. 2006).

The mechanical heating associated with radio mode accretion is assumed to impede, or even prevent, the cooling flow in central regions of the halo. More specifically, the radiated luminosity is taken to be

$$L_{\rm BH,R} = \epsilon_{\rm r} \dot{M}_{\rm BH,R} c^2, \quad (8)$$

where c is the speed of light and $\epsilon_{\rm r}$ describes how efficiently matter can be converted to energy near the event horizon. The standard value $\epsilon_{\rm r} = 0.1$ is adopted, which is an approximate value for radiatively efficient accretion onto a non-rapidly spinning black hole (Shakura & Syunyaev 1973). This injection of energy reduces the rate at which hot gas is able to cool onto the cold disk from $\dot{M}_{\rm cool}$ to $\dot{M}_{\rm cool} - 2L_{\rm BH}/v_{\rm vir}^2$, with the restriction that the cooling rate remains non-negative. The effectiveness of radio mode AGN feedback in suppressing cooling flows is greatest at late times and for large black hole masses, precisely what is required to reproduce the luminosities and colors of low-redshift, bright galaxies.

2.3. Hydrodynamical Simulations

To explore the effect of energy feedback from galaxies on the properties of the ICM, we couple the L-Galaxies SAM to hydrodynamical simulations. The initial conditions for these simulations are the same as those used for the two dark matter simulations described above, but we add gas particles with *zero* gravitational mass. The gas particles then act purely as "tracers" of the dark matter. In this way, we ensure that the dark matter distribution remains unaffected by the inclusion of baryons, so that the halo merger trees used to generate the semianalytic galaxy catalogs are the same.

Recent work has shown that the dissipative nature of the baryon fluid can have an influence on the structure of haloes (Stanek et al. 2009; Romano-Diaz et al. 2009; Pedrosa et al. 2009) and the growth of merger trees (Saro et al. 2008). However, all semianalytic modeling to date ignores such complications and uses merger trees based solely on the dark matter distribution. We are forced to follow this route so that we can use SAM input into our simulations. For the purposes of the results presented in this paper, the dark matter approximation is unlikely to make any significant difference to our conclusions.

The number of gas particles that we add is $N_{\rm gas} = 100^3$ for our small ($L = 62.5\ h^{-1}$ Mpc) simulation volume and $N_{\rm gas} = 200^3$ for our larger ($L = 125\ h^{-1}$ Mpc) volume. We choose to include gas at (approximately) the lower resolution of the Millennium Gas simulations[2] so that out technique remains computationally feasible when applied to the full Millennium volume in future work. In Section 4, we conduct a resolution test to demonstrate that increasing the resolution of the gas component relative to the dark matter has a negligible effect on our results.

The initial conditions are evolved from $z_{\rm i} = 127$ to $z = 0$ with a modified version of GADGET-2, designed to allow for gas particles with zero gravitational mass. Whenever a SPH calculation is to be done, we assume $\Omega_{\rm b,0} = 0.045$ and assign the gas particles their corresponding true mass: $m_{\rm gas} = 3.05 \times 10^9\ h^{-1}\ M_\odot$. This guarantees that gas properties such as density and entropy are computed correctly. In addition, gas particles are also given their true mass for simulation data dumps, with the mass of the dark matter particles accordingly reduced to $(1 - f_{\rm b}) m_{\rm DM} = 7.05 \times 10^8\ h^{-1}\ M_\odot$, where $f_{\rm b} = \Omega_{\rm b,0}/\Omega_{\rm m,0}$ is the mean cosmic baryon fraction.

In all of our hydrodynamical simulations, we choose to neglect gas cooling processes since radiative cooling, star formation, black hole growth, and associated feedback are incorporated in the SAM. Note, however, that gas particles are still converted to dissipationless "star" particles as dictated by the SAM, following the procedure outlined in Section 2.4.1 below.

We appreciate that the distribution and cooling of gas in haloes is treated in rather a simplistic manner in existing SAMs. However, we emphasize that, to the best of our knowledge, this is the *first* time the effect of energy feedback from galaxies on the ICM has been investigated using a SAM coupled to hydrodynamical simulations. As such, we believe it is sensible to begin with the simplest possible model where cooling is driven entirely by the SAM. In any case, the inclusion of gas cooling could only lead to a decrease in the entropy of intracluster gas, which would reinforce our conclusions with regard to the high degree of feedback that is required to explain the high entropy levels found in clusters.

A more self-consistent approach would be to include radiative cooling in our hydrodynamical simulations and use the gas distribution to inform the SAM. This extension of the semianalytic technique would require the simulation and the SAM to be coupled in such a way that both can be undertaken simultaneously. Extensive testing would be necessary to ensure that such a model was as successful as current SAMs in reproducing observed galaxy properties. Such a scheme is a long-term goal of our work but is beyond the scope of this paper.

The semianalytic galaxy catalogs that we have generated contain the positions and properties of all model galaxies at 64 redshift values, corresponding to the output times of our simulations. We have further modified GADGET-2 so that, once an output redshift is reached, temporary "galaxy" particles are introduced at the appropriate locations in the simulation volume. These galaxy particles have a set of associated properties, such as the change in stellar mass and energy released by SNe/AGNs since the last output, which are calculated from the SAM galaxy catalogs prior to the simulation. We use this information to form stars and heat gas in the neighborhood of each galaxy, as described in detail in the next section. Following star formation and the injection of energy, the galaxy particles are removed and the simulation progresses until the next output time, when the process is repeated.

Note that the properties of the ICM should not be affected by the frequency with which energy is injected as the time interval between our chosen 64 model outputs is always less than the galaxy halo dynamical time $t_{\rm dyn} = r_{\rm vir}/v_{\rm vir} = 0.1/H(z)$. We have verified that increasing the temporal resolution has a negligible effect on our results.

Cluster catalogs are constructed at $z = 0$ for our simulations using a procedure similar to that employed by Muanwong et al. (2002). Briefly, groups of dark matter particles are identified with the FOF algorithm, setting the linking length to be 10% of the mean interparticle spacing. A sphere is grown about the most gravitationally bound dark matter particle of each group until radii are found that enclose mean overdensities of $\Delta = 94$, $\Delta = 200$, $\Delta = 500$, $\Delta = 1000$, and $\Delta = 2500$, relative to the critical density $\rho_{\rm cr,0}$. Any clusters which overlap with a

[2] The Millennium Gas simulations (F. R. Pearce et al. 2009, in preparation) are a suite of large hydrodynamical simulations, all having the same volume as the Millennium simulation ($L = 500\ h^{-1}$ Mpc) and utilizing the same amplitudes and phases for the initial perturbations. The cosmological parameters are also identical, except that the present baryon density parameter $\Omega_{\rm b,0} = 0.045$ to reflect the inclusion of gas. The simulations contain $N_{\rm DM} = 1000^3/2$ dark matter and $N_{\rm gas} = 1000^3/2$ gas particles, with respective masses $1.42 \times 10^{10}\ h^{-1}\ M_\odot$ and $3.12 \times 10^9\ h^{-1}\ M_\odot$.

more massive system within these radii are discarded from the catalogs.

To check that dark matter structures are indeed undisturbed by the massless gas particles, we have compared the positions of cluster centers in catalogs generated from our dark matter-only simulation in the $L = 62.5\ h^{-1}$ Mpc box and a non-radiative hydrodynamical simulation in the same volume. At each overdensity Δ, we find that the distance between corresponding cluster centers in the two catalogs is less than the softening length for over 99% of our identified objects. We have also verified that this is the case at high redshift $z \approx 3$.

2.4. Implementing Star Formation and Feedback from Galaxies

2.4.1. Star Formation

Each model galaxy in the semianalytic catalogs has an associated stellar mass M_*. To compute the mass locked-up in stars formed over a redshift interval $\Delta z = z_{n+1} - z_n$, we take the stellar mass of the galaxy at z_n and subtract the sum of the stellar masses of its progenitors at the previous output z_{n+1}:

$$\Delta M_* = M_*(z_n) - \sum_{\text{prog.}} M_*(z_{n+1}). \quad (9)$$

Once an output redshift is reached in a simulation, we convert the $\Delta N_{\text{star}} = \Delta M_*/m_{\text{gas}}$ gas particles nearest to each model galaxy into collisionless star particles, reflecting the increase in stellar mass ΔM_* of the galaxy since the last output. To ensure that ΔN_{star} is an integer, we draw a random number r uniformly from the unit interval and compare it with the fractional part of ΔN_{star}: if r is less (greater) than the fractional part of ΔN_{star}, we round ΔN_{star} up (down) to the nearest integer. Note that the star particles also have zero gravitational mass, so they do not influence the dark matter distribution.

2.4.2. Type II Supernova Feedback

The energy released by Type II SNe between two successive outputs depends on the amount of mass that went into new stars during this time period. For each model galaxy, this is simply $\Delta m_* = \Delta M_*/(1-R)$, where ΔM_* is obtained from Equation (9). Inserting Δm_* into Equation (5) gives the mass of ejected gas, corresponding to an energy input into the ICM of

$$\Delta E_{\text{ejected}} = \frac{1}{2}\Delta m_{\text{ejected}} v_{\text{vir}}^2 \quad (10)$$

over the interval Δz. The solid line in Figure 1 shows the L-Galaxies prediction for the cumulative total energy transferred to the ICM by Type II SNe as a function of redshift. For comparison, the maximum possible total energy available from SNe is also shown as the dotted line. This is computed at each redshift by cumulatively summing ΔE_{SN} for all galaxies, assuming an efficiency $\epsilon_{\text{halo}} = 1$.

At each output, we distribute the available energy $\Delta E_{\text{ejected}}$ amongst the neighboring gas particles of a galaxy using a simple heating model. The basis of our model is that all gas within a distance r_{vir} of a galaxy can be heated by feedback processes in the time Δt between two outputs. We choose to inject energy in a distributed, rather than local, manner since, over a time Δt, heated gas will flow outward, mixing with infalling cooler gas at larger radii. We have also experimented with alternative heating models where each galaxy heats a fixed number of neighboring gas particles and found that our results are not significantly affected by the choice of heating model. In a forthcoming paper, we intend to investigate different ways of injecting energy into the ICM in more detail.

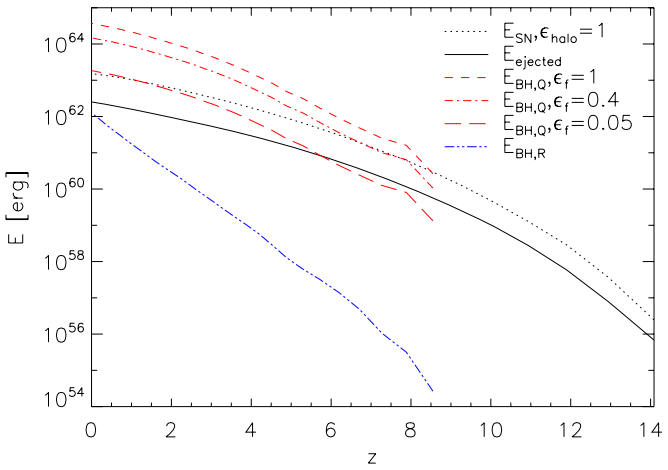

Figure 1. Cumulative total amount of energy transferred to the ICM by different feedback sources as a function of redshift in a box of side length $L = 62.5\ h^{-1}$ Mpc. The dotted line shows the total energy released by supernova explosions, while the solid line is the fraction of this energy available to heat intracluster gas. The contributions from quasar mode AGN feedback when the thermal coupling efficiency is $\epsilon_f = 1$, $\epsilon_f = 0.4$, and $\epsilon_f = 0.05$ are given by the dashed, dot-dashed, and long dashed lines, respectively. The triple-dot-dashed line shows the mechanical heating associated with radio mode accretion. However, in the Munich L-Galaxies semianalytic model, this energy only reduces the rate at which gas can cool out of the hot halo, rather than heating the ICM.

(A color version of this figure is available in the online journal.)

We implement our heating model in GADGET-2 as follows. For each galaxy, we find the number N_{ngb} of gas particles within a sphere of radius r_{vir} centered on the galaxy. If no neighbors are found, the search radius is increased until one gas particle is found. This is typically only necessary for low mass haloes. The energy released by SNe since the last output is then used to raise the entropy of the neighboring gas particles by a fixed amount

$$\Delta A_i = \frac{(\gamma - 1)\Delta E_{\text{ejected}}}{m_{\text{gas}} \sum_{j=1}^{N_{\text{ngb}}} [\max(f_{\text{b}}\rho_{\text{vir}}, \rho_j)]^{\gamma-1}}, \quad (11)$$

where $A = kT/(\mu m_{\text{p}} \rho^{\gamma-1})$ is the definition of entropy employed by GADGET-2, m_{p} is the mass of a proton, and $\mu \approx 0.6$ is the mean molecular weight for a fully ionized gas of primordial composition. By giving each particle a fixed entropy, rather than energy, boost, we ensure that denser particles close to the galaxy are heated to a higher temperature than more distant, lower density particles. The product of the cosmic baryon fraction f_{b} and the virial density ρ_{vir} gives the mean overdensity of baryons within the virial radius. If no neighbors are found within a distance r_{vir} of a galaxy and the search radius has to be increased until one particle is found, the density of this particle may be less than $f_{\text{b}}\rho_{\text{vir}}$. By using $[\max(f_{\text{b}}\rho_{\text{vir}}, \rho_j)]^{\gamma-1}$, rather than $\rho_j^{\gamma-1}$, in the sum in Equation (11), we are assuming that the amount of energy used to heat such particles is $\Delta E_{\text{ejected}}(\rho_i/f_{\text{b}}\rho_{\text{vir}})^{\gamma-1} < \Delta E_{\text{ejected}}$; the rest of the energy is taken to be used up as the gas does work expanding adiabatically to a density $\rho_i < f_{\text{b}}\rho_{\text{vir}}$.

2.4.3. Feedback from Active Galactic Nuclei

A similar approach is used to calculate the energy released by AGN activity over a redshift interval Δz. For each galaxy, the total change in mass of the central black hole ΔM_{BH} is given by

Equation (9), but with M_* replaced by $M_{\rm BH}$. The fraction of this mass accreted via the radio mode is approximately

$$\Delta M_{\rm BH,R} = \dot{M}_{\rm BH,R}\Delta t, \quad (12)$$

where $\dot{M}_{\rm BH,R}$ is obtained by evaluating Equation (7) at the current output z_n. It follows that the mass change due to merger-driven accretion is then

$$\Delta M_{\rm BH,Q} = \Delta M_{\rm BH} - \Delta M_{\rm BH,R}. \quad (13)$$

We ensure that the radiated luminosity

$$L_{\rm BH,Q} = \epsilon_{\rm r}\dot{M}_{\rm BH,Q}c^2 \quad (14)$$

does not exceed the Eddington luminosity

$$L_{\rm Edd} = 1.3 \times 10^{38}\left(\frac{M_{\rm BH}}{M_\odot}\right)\ {\rm erg\ s^{-1}} \quad (15)$$

(e.g., Begelman & Meier 1982) when averaged over the time Δt between two successive outputs. We then assume that some fraction of the energy radiated during quasar mode accretion is coupled thermally to the ICM:

$$\Delta E_{\rm BH,Q} = \epsilon_{\rm f} L_{\rm BH,Q}\Delta t, \quad (16)$$

where the coupling efficiency $\epsilon_{\rm f}$ is a free parameter; we discuss suitable values for this parameter in the following section. The dashed, dot-dashed, and long dashed lines in Figure 1 show the cumulative total energy transferred to the ICM by quasar mode AGN feedback for the cases $\epsilon_{\rm f} = 1$, $\epsilon_{\rm f} = 0.4$, and $\epsilon_{\rm f} = 0.05$, respectively. We inject the energy $\Delta E_{\rm BH,Q}$ released by quasar mode accretion into gas particles surrounding model galaxies using the same heating model as for supernova feedback.

The mechanical heating

$$\Delta E_{\rm BH,R} = \epsilon_{\rm r}\Delta M_{\rm BH,R}c^2 \quad (17)$$

associated with quiescent accretion simply reduces the rate at which gas in the hot halo cools onto the disk. In other words, radio mode feedback does not explicitly heat intracluster gas within the framework of L-Galaxies and is thus irrelevant for our hybrid approach. For completeness, we show the cumulative total energy liberated by radio mode accretion as the triple-dot-dashed line in Figure 1.

3. RESULTS AND DISCUSSION

3.1. Model Discrimination

One of the most fundamental properties of galaxy groups and clusters is the X-ray luminosity–temperature relation. Only recently have self-consistent hydrodynamical simulations been able to successfully reproduce the slope and normalization of this relation over a wide range of mass scales. In this section, we explore the individual effects of stellar and AGN feedback on the $L_{\rm X}$–T relation with a set of test simulations performed in the $L = 62.5\ h^{-1}$ Mpc box using our hybrid technique.

3.1.1. Star Formation and Supernova Feedback

As a starting point, we include only star formation and associated supernova feedback as predicted by L-Galaxies. Figure 2 shows our simulated groups and clusters on the $L_{\rm X}$–T plane at $z = 0$, shaded by their hot gas fraction. Bolometric

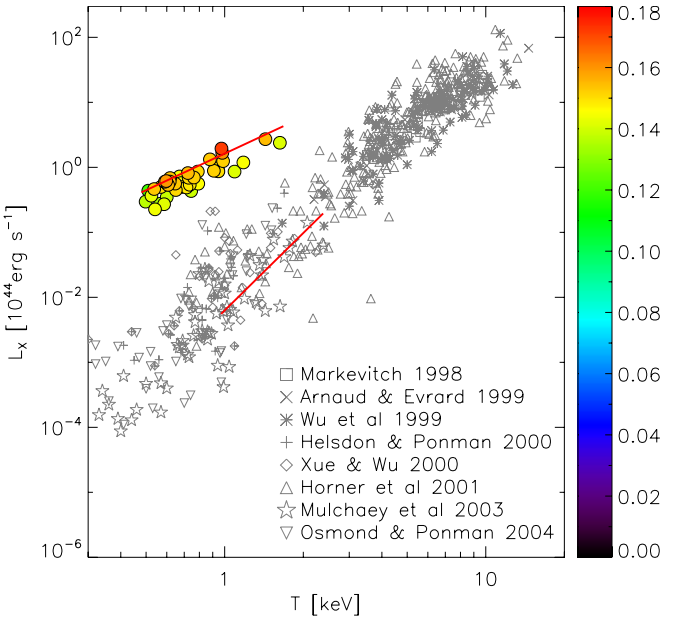

Figure 2. Bolometric X-ray luminosity as a function of emission-weighted temperature for groups and clusters formed in a hybrid simulation with L-Galaxies star formation and Type II supernova feedback. X-ray properties are computed within r_{500} and each object is shaded according to its hot gas fraction. For comparison, the upper and lower solid lines are the best-fit relations from non-radiative and preheating simulations, respectively. Several data sets obtained from X-ray observations of groups and clusters are also shown.

(A color version of this figure is available in the online journal.)

X-ray luminosities and emission-weighted temperatures were computed using the procedure outlined by Muanwong et al. (2002). Since radiative cooling is neglected in our simulations, we do not anticipate excess emission in cluster cores due to strong cooling flows and it is therefore unnecessary to remove emission from central regions. All cluster properties are calculated within r_{500} since $\Delta = 500$ is typically the smallest density contrast accessible to observations. Furthermore, we only consider galaxy groups and clusters with a mass $M_{500} \geqslant 1.3 \times 10^{13}\ h^{-1}\ M_\odot$, corresponding to a total of about 15,000 particles within r_{500}. The most massive object formed has a mass $M_{500} \approx 7 \times 10^{13}\ h^{-1}\ M_\odot$.

For comparative purposes, data from a number of X-ray observational studies is shown (Markevitch 1998; Arnaud & Evrard 1999; Wu et al. 1999; Helsdon & Ponman 2000; Xue & Wu 2000; Horner 2001; Mulchaey et al. 2003; Osmond & Ponman 2004). The uppermost solid line in Figure 2 is the best-fit $L_{\rm X}$–T relation obtained from a simulation that includes gravitational heating only. We find that $L_{\rm X} \propto T^{1.91\pm0.37}$ in this case, close to the $L_{\rm X} \propto T^2$ scaling predicted by theoretical arguments. The lower solid line shows the best-fit $L_{\rm X}$–T relation for a simulation with uniform preheating at high redshift. The preheating model adopted imposes an entropy floor $S_{\rm preheat} = 200$ keV cm^2 at $z = 4$. Preheating leads to a much steeper relation: $L_{\rm X} \propto T^{3.87\pm0.87}$, consistent with observational data.

Observe that nearly all of our data points lie just below the best-fit $L_{\rm X}$–T relation for the gravitational heating simulation, with only a slight hint of steepening. The hot gas fractions of our groups and clusters are at least 65% of the cosmic baryon fraction, with some having a hot gas fraction very close to $f_{\rm b}$. Observational data suggests that only massive clusters ($T \gtrsim 5$ keV) have such large gas fractions, with groups and poor clusters typically having much smaller gas fractions (Sanderson

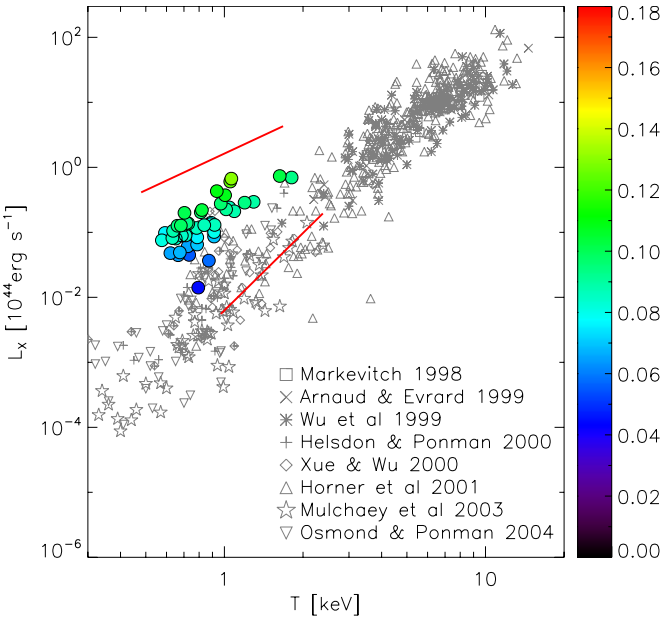

Figure 3. Same as Figure 2, but with an enhanced stellar feedback scheme in which the L-Galaxies star formation efficiency is 5 times greater and the amount of energy transferred to the ICM by Type II SNe has been set to its maximum possible value.

(A color version of this figure is available in the online journal.)

et al. 2003; Vikhlinin et al. 2006; Sun et al. 2009). These results indicate that the entropy of the ICM has been raised by stellar feedback, but nowhere near enough to explain observed X-ray luminosities.

By contrast, hydrodynamical simulations with radiative cooling, star formation, and supernova feedback tend to produce a closer match to the observed L_X–T relation (e.g., Borgani et al. 2004; Puchwein et al. 2008). There are two reasons for this. First, the amount of baryons that cool and form stars is typically much greater in hydrodynamical simulations, with 30%–50% of the baryons within the virial radius locked-up in stars (e.g., Balogh et al. 2001; Davé et al. 2002; Tornatore et al. 2003). In our hybrid simulation, the average stellar fraction within the virial radius is approximately 9%, in agreement with observational data (Balogh et al. 2001; Lin et al. 2003; Balogh et al. 2008). This is, of course, to be expected since star formation in our simulation is driven by a SAM which has been tuned to reproduce the cosmic star formation history. Second, popular stellar feedback schemes typically assume that each supernova event transfers more energy to the surrounding gas. For example, in the models of Springel & Hernquist (2003) and Kay et al. (2004), the amount of energy returned to the ICM per solar mass of stars formed is at least 4×10^{48} erg $M_\odot^{-1}$. Within the framework of L-Galaxies, it follows from Equation (5) that this is only possible if no energy is used to reheat cold disk gas ($\Delta E_{\rm hot} = 0$) and the efficiency parameter $\epsilon_{\rm halo} = 1$.

To test that our method yields comparable results to existing hydrodynamical simulations when the star formation efficiency is increased, we have performed a simulation where the mass of newly formed stars Δm_* is simply multiplied by 5. We also assume the energy imparted to the ICM by SNe is larger: $\Delta E_{\rm ejected} = \Delta E_{\rm SN}$, with an efficiency $\epsilon_{\rm halo} = 1$. Note that setting $\Delta E_{\rm hot} = 0$ means all star-forming galaxies can eject gas from their halo, rather than just those with a virial velocity $v_{\rm vir} \lesssim 200$ km s^{-1}. Figure 3 shows the resulting L_X–T relation. It is evident that cluster X-ray luminosities and hot gas fractions are significantly reduced relative to those predicted by the standard L-Galaxies stellar feedback model. Our results are in broad agreement with those obtained from simulations incorporating star formation and supernova feedback (e.g., Borgani et al. 2004; Puchwein et al. 2008). However, the normalization of the L_X–T relation is still too high and the slope is too shallow relative to the observed relation. The stellar fraction within the virial radius has now increased to 39% on average, conflicting with observations but again similar to results from direct simulations (e.g., Puchwein et al. 2008).

The heating of intracluster gas by stellar feedback from model galaxies is clearly insufficient to reproduce the L_X–T relation, particularly on group scales. This remains the case even when the star formation efficiency is unrealistically high. Even if we were to allow for the energy released by Type Ia SNe, this is unlikely to bring the L_X–T relation shown in Figure 2 in line with observations since the energetics of Type Ia and Type II SNe are thought to be roughly similar. However, Type Ia SNe are crucially important for chemically enriching the ICM at low redshift (e.g., Mannucci et al. 2005); an issue we shall address elsewhere. We now investigate whether additional energy input from AGNs can resolve this problem, starting with feedback from quasar-induced outflows.

3.1.2. Including Feedback from Active Galactic Nuclei

Cosmological simulations including prescriptions for black hole growth and associated quasar activity have been performed by Di Matteo et al. (2008). They assumed 5% of the energy radiated during quasar mode accretion is coupled thermally and isotropically to the surrounding medium. This choice ensures that the normalization of the local black hole–bulge mass relation agrees with observations (Di Matteo et al. 2005). In their model, the radiated luminosity is related to the total black hole accretion rate $\dot{M}_{\rm BH}$, whereas we assume it is governed by the merger-driven accretion rate $\dot{M}_{\rm BH,Q}$. However, the growth of black holes in L-Galaxies is dominated by quasar mode accretion, so that $\Delta M_{\rm BH} \approx \Delta M_{\rm BH,Q}$ anyway. Based on this argument, it seems sensible to begin by setting $\epsilon_{\rm f} = 0.05$ in Equation (16).

Figure 4 shows the L_X–T relation obtained from a hybrid simulation including star formation, supernova and quasar mode AGN feedback with a coupling efficiency $\epsilon_{\rm f} = 0.05$. Again, cluster X-ray luminosities and hot gas fractions are considerably over-estimated. Di Matteo et al. (2008) did not use their model to investigate the L_X–T relation of groups and clusters. However, since the global black hole accretion rate histories in L-Galaxies and the simulations of Di Matteo et al. (2008) are similar, we would expect them to obtain a similar result.

In order to recover the observed steepening of the L_X–T relation on group scales, we find that the quasar mode coupling efficiency has to be increased to $\epsilon_{\rm f} = 0.4$. The L_X–T relation in this case is shown in Figure 5. Our simulated clusters now provide a much better match to the observational data. In addition, the gas fractions of our clusters are in broad agreement with observations (Sanderson et al. 2003; Sun et al. 2009).

Artificially boosting the feedback from merger-driven accretion can be viewed as a crude attempt at including radio mode feedback since, at each redshift, over 75% of model galaxies with a central black hole accrete via both modes. Can we recover the correct L_X–T relation by explicitly including the radio mode contribution, rather than simply increasing $\epsilon_{\rm f}$? Recall that the L-Galaxies implementation of radio mode feedback only reduces the rate at which gas can cool out of the quasi-static hot halo, rather than directly heating the ICM. Even if we

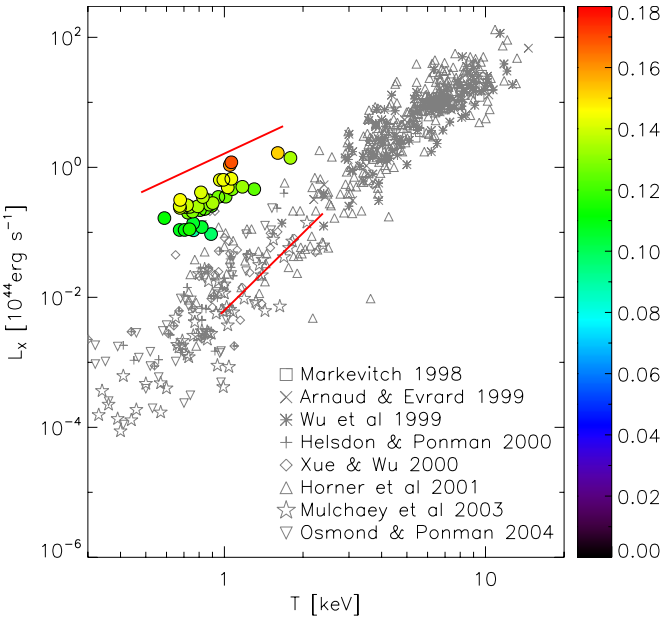

Figure 4. Same as Figure 2, but for a hybrid simulation with L-Galaxies stellar feedback and a simple model for quasar mode AGN feedback. The energy released by merger-driven accretion onto the central black hole is assumed to be thermally coupled to the intracluster gas with an efficiency $\epsilon_f = 0.05$.

(A color version of this figure is available in the online journal.)

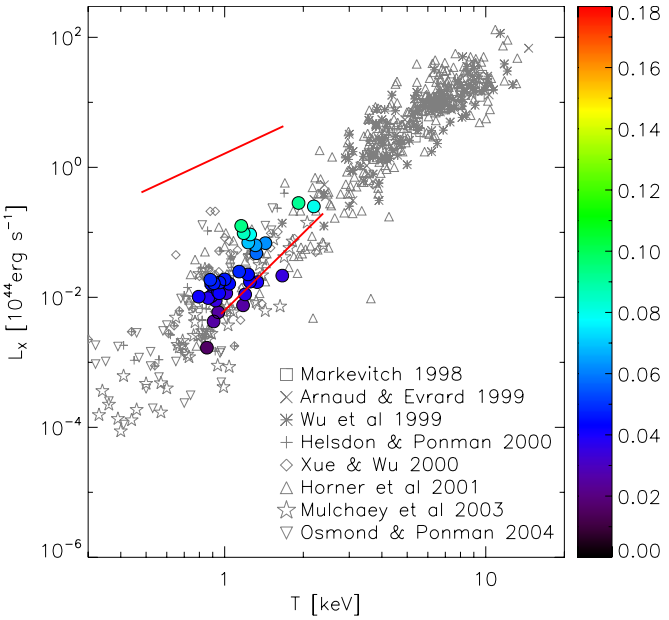

Figure 5. Same as Figure 4, except the thermal coupling efficiency for quasar mode AGN feedback has been increased to $\epsilon_f = 0.4$.

(A color version of this figure is available in the online journal.)

temporarily ignore this feature of the model and inject all of the energy $\Delta E_{BH,R}$ (see Equation (17)) released by quiescent accretion into the gas component of a simulation incorporating stellar and quasar mode feedback with $\epsilon_f = 0.05$, we find that it has little effect on the L_X–T relation shown in Figure 4. This is because the mechanical heating associated with radio mode accretion is negligible at high redshift, only becoming comparable to the energy released by SNe at $z = 0$; see Figure 1. However, Puchwein et al. (2008) have successfully reproduced the observed mean L_X–T relation by incorporating a model for AGN-driven bubble heating into the quasar mode feedback scheme of Di Matteo et al. (2008). This highlights the need for an alternative model of AGN feedback in which the radio mode does more than just offset cooling from the hot halo.

In recent work, Bower et al. (2008) have used the Durham SAM GALFORM to investigate the properties of the ICM, particularly the L_X–T relation. They demonstrated that the version of the model developed by Bower et al. (2006) overpredicts X-ray luminosities on group scales, leading to a shallow L_X–T relation similar to the one we obtained from our simulation with L-Galaxies stellar feedback (Figure 2). In this model, the energy released by quiescent radio mode accretion simply prevents any significant amount of gas cooling in massive haloes, as in L-Galaxies. To try to explain the X-ray properties of galaxy groups and clusters whilst simultaneously accounting for the observed properties of galaxies, Bower et al. (2008) proposed a modification of GALFORM which allows for heat input into the ICM from radio mode feedback. This additional heating acts to expel gas from the X-ray emitting central regions of haloes, reducing the gas density and thus luminosity. Lower-mass systems are affected more than massive ones because their cooling time is shorter, meaning they initially supply more material to the central black hole, resulting in a larger amount of feedback per unit mass of gas. The L_X–T relation then becomes steeper as desired on group scales. With this modification, the GALFORM model reproduces the observed mean L_X–T relation and the substantial scatter about this relation at low temperatures ($T \lesssim 3$ keV), as well as halo gas fractions (Bower et al. 2008).

The basis of the Bower et al. (2008) AGN feedback model is to compute the heating power L_{heat} as a function of the cooling rate. More specifically,

$$L_{heat} = \eta_{SMBH} \epsilon_r \dot{M}_{cool} c^2, \quad (18)$$

subject to the constraint

$$L_{heat} \leqslant \epsilon_{SMBH} L_{Edd}. \quad (19)$$

Here, $\dot{M}_{cool}$ is the cooling rate of the halo in the absence of radio mode feedback, related to the black hole accretion rate via $\dot{M}_{BH} = \eta_{SMBH} \dot{M}_{cool}$. The parameter η_{SMBH} controls the efficiency with which cooling material can be accreted by the black hole and is set to $\eta_{SMBH} = 0.01$ by Bower et al. (2008). The limiting criterion in Equation (19) relates to the structure of the accretion disk itself. Effective radio mode feedback requires efficient jet production, typically thought to be associated with geometrically thick, advection dominated disks (e.g., Rees et al. 1982; Meier 2001; Churazov et al. 2005). If the accretion rate is too high, models suggest that the vertical height of the disk will collapse, leading to a drop in jet production efficiency. Much more of the energy released by accretion is then radiated away and is not available for radio mode feedback. Based on theoretical work (e.g., Esin et al. 1997), Bower et al. (2008) assume this change in structure of the accretion disk occurs once the accretion rate reaches $\dot{M}_{BH} = \epsilon_{SMBH} \dot{M}_{Edd}$, where ϵ_{SMBH} is referred to as the disk structure parameter and is related to the disk viscosity parameter α by $\epsilon_{SMBH} \propto \alpha^2$. The disk structure parameter is assigned a value $\epsilon_{SMBH} = 0.02$, in accordance with plausible accretion disk viscosities (e.g., McKinney & Gammie 2004; Hirose et al. 2004; Hawley & Krolik 2006). Note that the AGN feedback model suggested by Sijacki et al. (2007) also assumes that radio mode feedback is only effective for accretion rates below some fraction of the Eddington rate.

The heating energy available from the AGN is compared with the energy lost radiatively by gas cooling from the halo. If the

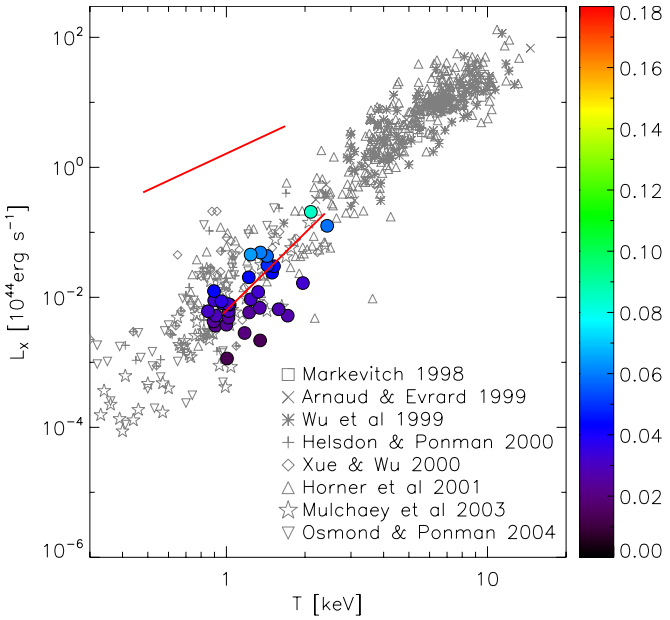

Figure 6. Same as Figure 2, but for a hybrid simulation with L-Galaxies stellar feedback and the Bower et al. (2008) AGN feedback prescription employed in the latest version of GALFORM.

(A color version of this figure is available in the online journal.)

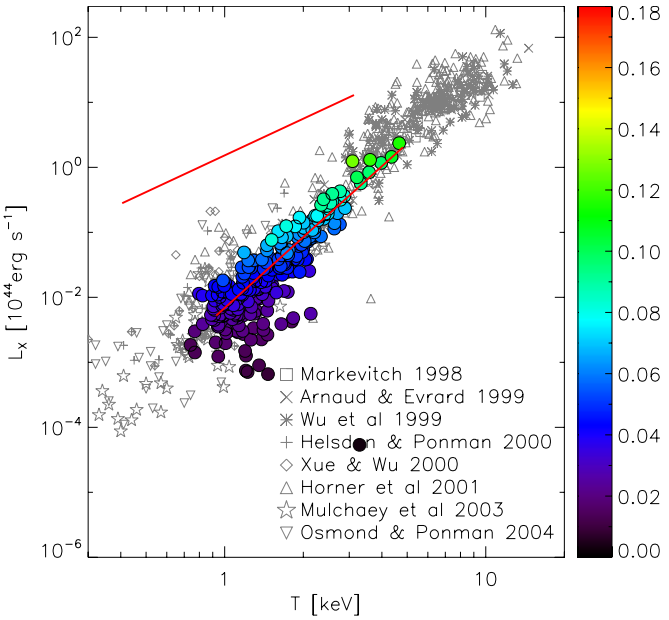

Figure 7. Bolometric X-ray luminosity as a function of emission-weighted temperature for a hybrid simulation with our best-fit feedback model. This model consists of stellar feedback from L-Galaxies combined with the Bower et al. (2008) AGN feedback prescription. See the caption of Figure 2 for a description of the shading and best-fit lines.

(A color version of this figure is available in the online journal.)

feedback energy is greater than the radiated energy, the excess energy is used to eject gas from the halo. The energy transferred to the ICM over a time period Δt is then

$$\Delta E_{\rm ejected} = \Delta E_{\rm heat} - \Delta E_{\rm cool}, \quad (20)$$

where $\Delta E_{\rm heat} = L_{\rm heat}\Delta t$ and

$$\Delta E_{\rm cool} = \frac{1}{2}\Delta M_{\rm cool} v_{\rm vir}^2. \quad (21)$$

We have implemented the Bower et al. (2008) prescription for AGN feedback in our hybrid approach using the following procedure. For each galaxy in the catalog, we take the total change in black hole mass between two successive outputs, $\Delta M_{\rm BH}$, and compute $\Delta M_{\rm cool} = \Delta M_{\rm BH}/\eta_{\rm SMBH}$. Inserting this into Equations (18) and (21) gives $\Delta E_{\rm heat}$ and $\Delta E_{\rm cool}$, respectively. The heat input into the ICM from each model galaxy then follows from Equation (20). This energy is injected into the gas component of our simulation using the same heating model as described previously.

To be fully consistent, we should take into account the effect of AGN heating on hot halo gas within L-Galaxies itself. As in Bower et al. (2008), this would almost certainly lead to changes in some of the other model parameters. However, if we were to adjust the appropriate parameters so as to regain a realistic galaxy population, then we would require galaxy properties (particularly their black hole masses) to be similar to those in our existing galaxy catalog. The amount of heating energy available from AGNs would then also be (approximately) the same since it is driven purely by the black hole growth rate in the Bower et al. (2008) model.

Figure 6 shows the L_X–T relation obtained from a simulation with L-Galaxies stellar feedback and the AGN feedback model of Bower et al. (2008). Our results clearly provide an excellent match to the observational data. In addition, the hot gas and stellar fractions of our groups and clusters agree with observed values. This success indicates that the L-Galaxies implementation of AGN feedback must indeed be revised if the model is to explain the observed properties of both the galaxy distribution and the ICM.

3.2. Best-fit Model

Following the analysis presented in the preceding section, we have established a model that is capable of reproducing the observed L_X–T relation of groups and poor clusters. This best-fit model comprises of the stellar feedback scheme employed in L-Galaxies, combined with the AGN feedback prescription of Bower et al. (2008). To investigate whether this model can also correctly explain the properties of richer clusters, we have performed a hybrid simulation in a larger $L = 125\ h^{-1}$ Mpc volume.

3.2.1. The X-ray Luminosity–Temperature Relation

The $z = 0$ L_X–T relation obtained from our simulation is shown in Figure 7. Groups and clusters are shaded by their hot gas fraction and we only plot clusters with a mass $M_{500} \geqslant 1.3 \times 10^{13}\ h^{-1}\ M_\odot$. The mass of the largest cluster formed is now $M_{500} \approx 2.3 \times 10^{14}\ h^{-1}\ M_\odot$. For comparison, we show the best-fit L_X–T relations from a non-radiative simulation (upper solid line) and a simulation with the same preheating model as described previously (lower solid line). These relations are of the form $L_X \propto T^{1.88\pm0.16}$ and $L_X \propto T^{3.62\pm0.33}$, respectively. As before, our hybrid simulation yields an L_X–T relation with a slope and normalization that is generally consistent with observations at all mass scales. A few objects appear to have a higher temperature than expected, given their X-ray luminosity. This is particularly true for the $T \approx 3.3$ keV cluster with a luminosity $L_X \approx 5.4 \times 10^{39}$ erg s^{-1}. The reason for this is that the gas in this object has recently been raised to a high temperature by a large energy injection from the central AGN, causing it to flow outward. As this gas is replaced by infalling cooler gas, the system will stabilize and shift back toward the main relation. Our results exhibit a variation in scatter along the

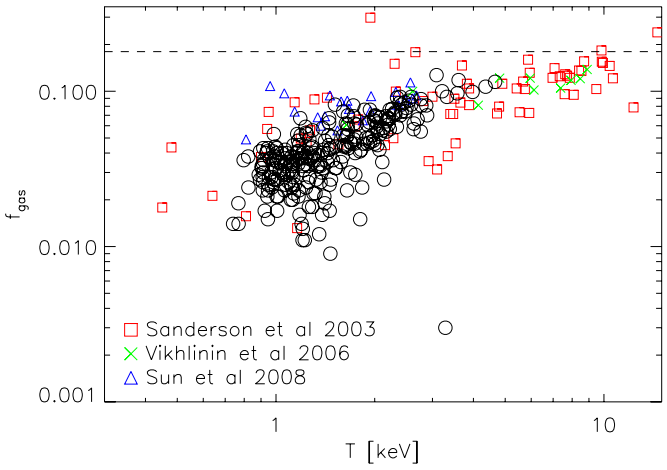

Figure 8. Halo hot gas fraction within r_{500} as a function of emission-weighted temperature for a hybrid simulation with our best-fit feedback model. Simulated objects are shown by the open circles. A variety of data from X-ray observations of groups and clusters is shown for comparison. The horizontal dashed line is the mean cosmic baryon fraction, f_b, in the cosmological model we have adopted.

(A color version of this figure is available in the online journal.)

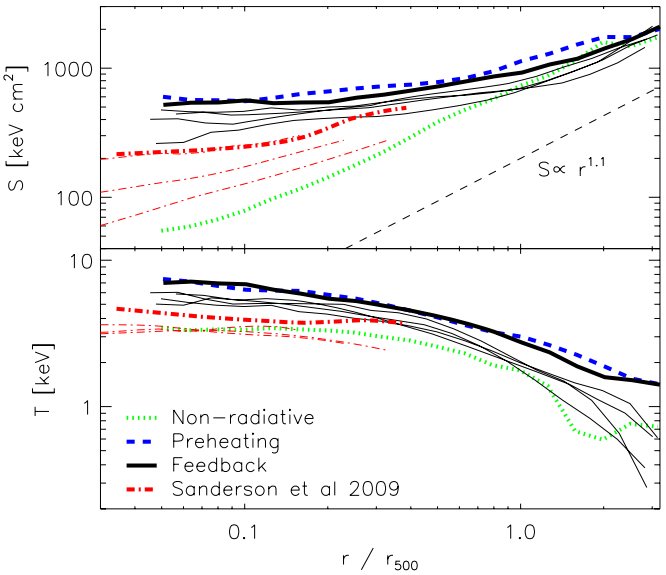

Figure 9. Radial profiles of entropy (upper panel) and emission-weighted temperature (lower panel) obtained from a hybrid simulation with our best-fit feedback model. The solid lines are profiles for a sample of five clusters with a mass $1.1 \times 10^{14}\ h^{-1}\ M_\odot \leqslant M_{500} \leqslant 1.7 \times 10^{14}\ h^{-1}\ M_\odot$, with the profiles of the most massive cluster in this sample highlighted by thick solid lines. For comparative purposes, the thick dotted and dashed lines are the profiles of the corresponding object formed in a non-radiative and a preheating simulation, respectively. In addition, observed profiles for four non-cool core clusters from the sample presented by Sanderson et al. (2009) are shown as thin dot-dashed lines. These objects are of similar mass to our simulated clusters: $1.1 \times 10^{14}\ h^{-1}\ M_\odot \leqslant M_{500} \leqslant 1.6 \times 10^{14}\ h^{-1}\ M_\odot$, and the thick dot-dashed lines highlight the profiles of the most massive object. Theoretical arguments predict that entropy scales as $S \propto r^{1.1}$ outside of cluster cores, shown by the thin dashed line in the upper panel.

(A color version of this figure is available in the online journal.)

L_X–T relation that is similar to observational data. In particular, for temperatures $T \lesssim 3$ keV, our data points fan out to populate a triangular region of the L_X–T plane in the same way. This scatter about the low-temperature end of the L_X–T relation is attributable to the variety of merger histories of groups. Note that there seems to be more scatter toward the lower-luminosity edge of the observed relation than the upper-luminosity edge. This is because we cannot produce systems with a highly X-ray luminous CC in our simulations since we have chosen to neglect cooling processes (see Section 3.2.3).

3.2.2. Halo Gas Fractions

It is evident from Figure 7 that, as we move along the L_X–T relation from group to cluster scales, the hot gas fraction of our simulated objects increases, reaching approximately 70% of the mean cosmic baryon fraction in massive clusters. To illustrate this behavior more clearly, we explicitly plot the hot gas fraction f_{gas} as a function of emission-weighted temperature (both within r_{500}) in Figure 8. For comparative purposes, we show constraints on halo gas fractions obtained from X-ray observations (Vikhlinin et al. 2006; Sun et al. 2009). Also plotted are gas fractions within r_{500} computed from the gas density and temperature profile parameters given in Sanderson et al. (2003).

The gas fractions of our groups and clusters are in broad agreement with the observational data, exhibiting a comparable amount of scatter. In both our results and the data, we see a rapid decline in gas fraction at lower temperatures. This is because AGN feedback is effective at driving gas from the central regions of low-mass systems. On the other hand, the potential wells of massive clusters are too deep for AGN heating to efficiently remove gas from them, so they retain a much larger fraction of their hot gas. Finally, we note that the $T \approx 3.3$ keV cluster with the smallest gas fraction (0.3%) corresponds to the system in Figure 7 with $L_X \approx 5.4 \times 10^{39}$ erg s^{-1} discussed before. This supports our argument that this object has recently experienced an intense burst of AGN activity which has driven a substantial amount of gas beyond r_{500}.

3.2.3. Entropy and Temperature Profiles

Further information about non-gravitational heating processes operating in clusters can be gleaned by inspecting radial entropy and temperature profiles of the ICM. In the upper (lower) panel of Figure 9, the thin solid lines are entropy (emission-weighted temperature) profiles for a sample of five of our most massive clusters, with masses in the range $1.1 \times 10^{14}\ h^{-1}\ M_\odot \leqslant M_{500} \leqslant 1.7 \times 10^{14}\ h^{-1}\ M_\odot$ at $z = 0$. Thick solid lines highlight the profiles of the most massive cluster in this sample (the second most massive object in the simulation volume). For reference, the thick dotted and dashed lines are the profiles of the corresponding object formed in the non-radiative and preheating simulations, respectively. Profiles are only plotted for radii greater than the gravitational softening length. In addition, observed profiles for four NCC clusters from the sample presented by Sanderson et al. (2009) are shown as thin dot-dashed lines. These objects are of similar mass to our simulated clusters: $1.1 \times 10^{14}\ h^{-1}\ M_\odot \leqslant M_{500} \leqslant 1.6 \times 10^{14}\ h^{-1}\ M_\odot$, with the profiles of the most massive object highlighted by thick dot-dashed lines. We only compare our profiles with those of NCC clusters since our simulations are non-radiative and thus systems with a CC do not form.

Theoretical models of shock heating during spherical collapse predict that entropy scales with radius as $S \propto r^{1.1}$ (e.g., Tozzi & Norman 2001). This scaling behavior is indeed observed in cluster outskirts, but entropy profiles are typically seen to become flatter in central regions $r \lesssim 0.2 r_{200}$ (e.g., Ponman et al. 2003; Pratt et al. 2006). However, the precise radius at which this flattening occurs varies considerably, depending on such factors as the temperature (mass) of the system and whether it has a CC or a NCC. In particular, hotter, more massive objects have a higher mean core entropy (e.g., Cavagnolo et al. 2009),

and the profiles of NCC clusters flatten off at significantly larger radii than those of CC clusters (e.g., Sanderson et al. 2009).

The power-law $S \propto r^{1.1}$ is illustrated by the thin dashed line in the upper panel of Figure 9 (the normalization is arbitrary). It is evident that the entropy profiles of our clusters depart from this scaling at somewhat larger radii than observed: $r \approx r_{500}$, flattening as we move in toward the core and overestimating the central entropy. Likewise, the temperature profiles shown in the lower panel of Figure 9 reveal that the core temperature is higher than would be expected for objects of this mass. This is similar to the behavior predicted by the preheating model, although our feedback model yields an entropy profile that provides a slightly better match to the observational data.

Based on the preceding discussion it is natural to ask how we can recover the observed L_X–T relation and halo gas fractions within r_{500} if the gas entropy is overestimated in cluster cores. The answer lies in the fact that the full Sanderson et al. (2009) sample contains clusters with a variety of entropy profiles. If we consider the emission per unit logarithmic radius, $dL_X/d\log_{10} r$, the most centrally concentrated CC clusters have their peak emission within $0.2r_{500}$, whereas in some NCC clusters the peak is beyond $0.7r_{500}$. Our most massive simulated clusters resemble these latter objects, and hence lie at the lower-luminosity edge of the L_X–T relation (for low-mass systems, the observations do not extend far enough in radius to make a meaningful comparison).

We note that profiles can only be reliably measured for groups and poor clusters that are very X-ray bright. However, optically selected samples of groups have revealed systems with little or no detectable X-ray emission that may be the group analogue of NCC clusters (e.g., Rasmussen et al. 2006). It may not be possible to extract profiles for such objects, but since they are X-ray underluminous we would expect them to have a large entropy core, possibly similar to that seen in the profiles of our simulated groups.

However, in order to reproduce the observed profiles of the majority of X-ray bright groups and poor clusters, the entropy and temperature of the gas in core regions must be lowered. This could potentially be achieved by incorporating cooling processes in our simulations. The inclusion of radiative cooling would only strengthen our conclusion that large amounts of energy must be injected into the ICM by AGNs to recover the observed L_X–T relation and halo gas fractions.

4. RESOLUTION TEST

In all of the hydrodynamical simulations presented in this paper we have chosen a lower resolution for the gas component than for the dark matter. To check that this approach yields robust results, we have performed a suite of six hybrid simulations in the $L = 62.5\ h^{-1}$ Mpc box with a fixed number $N_{DM} = 270^3$ of dark matter particles, but different numbers of gas particles. Two of these simulations have $N_{gas} < 100^3$, while for the other three $N_{gas} > 100^3$ (recall that all our simulations in this volume have $N_{gas} = 100^3$). All other simulation parameters are unchanged between the runs. The feedback scheme we adopt is our best-fit model since this is the only one that we have used in the larger $L = 125\ h^{-1}$ Mpc box and it is this model we intend to apply in the future.

To demonstrate that $N_{gas} = 100^3$ is a sufficient number of gas particles for a converged estimate of the L_X–T relation, in Figure 10 we compare the relations obtained from three simulations with $N_{gas} = 50^3$, $N_{gas} = 100^3$ and $N_{gas} = 200^3$, respectively. The corresponding (true) masses of the gas particles are

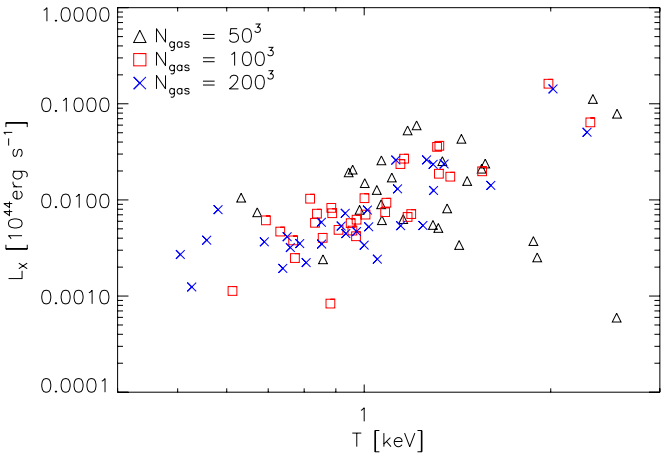

Figure 10. Bolometric X-ray luminosity as a function of emission-weighted temperature for three hybrid simulations with our best-fit feedback model. To demonstrate the effect of resolution, the simulations are identical in all aspects except for the number of gas particles used, as detailed in the legend.

(A color version of this figure is available in the online journal.)

then $m_{gas} = 2.44 \times 10^{10}\ h^{-1}\ M_\odot$, $m_{gas} = 3.05 \times 10^{9}\ h^{-1}\ M_\odot$, and $m_{gas} = 3.81 \times 10^{8}\ h^{-1}\ M_\odot$. X-ray luminosities and emission-weighted temperatures are computed within r_{500} and only objects with a mass $M_{500} \geqslant 1.3 \times 10^{13}\ h^{-1}\ M_\odot$ are plotted. Focusing on the two most massive clusters, we see that they have very similar temperatures and luminosities in the intermediate and high-resolution runs. We find that this remains the case if we go to even higher resolution. However, they shift significantly in the low-resolution simulation. This signifies numerical convergence at the intermediate resolution for systems with $T \gtrsim 2$ keV, which is important since we plan to use our technique to preferentially study rich clusters in subsequent work.

As we move to lower temperatures, the amount of scatter between the three different resolution simulations increases. In the low resolution run, the data points are less tightly grouped and seem to lie on a mean relation that has a shallower slope than in the other two simulations. In addition, three objects have anomalously high temperatures given their X-ray luminosity. This is because there is a limited number of gas particles available for heating in these low-mass systems at this resolution and a large amount of energy has recently been injected into a small number of gas particles. On the other hand, the groups and clusters formed in the intermediate and high-resolution runs lie on a similar mean relation, although the data points do not line-up perfectly. This indicates that we have not attained numerical convergence at the lowest resolution. Note that the L_X–T relation in the intermediate and high-resolution runs appears to flatten slightly at the low temperature end in the same way as observational data.

It is not surprising that we do not achieve exact convergence for two reasons. First, in situations where only one gas particle is heated, it is evident from Equation (11) that the entropy boost given to the particle is inversely proportional to its (true) mass: $\Delta A_i \propto 1/m_{gas}$, if its density is less than $f_b\rho_{vir}$. Consequently, as the resolution is increased, the particle will receive a larger entropy injection. Second, there is a stochastic element to our star formation scheme. By performing another intermediate-resolution simulation with a different random seed, we found that this randomness induces considerable scatter in the luminosities and temperatures of the lowest-mass systems, but has little effect in more massive objects. Based on these considerations, we suggest that the X-ray properties computed

for groups with $T \lesssim 1$ keV are unreliable since these systems contain relatively few gas particles. However, we feel that the level of convergence between the intermediate and high-resolution runs for objects with $T \gtrsim 1$ keV is sufficient to give a good statistical representation of the net effect of feedback on the L_X–T relation.

5. SUMMARY AND CONCLUSIONS

In this paper, we set out to extend the predictive power of current SAMs of galaxy formation by investigating the effect of energy feedback from model galaxies on the properties of intracluster gas. To achieve this objective we have employed a novel hybrid technique in which a SAM is coupled to non-radiative hydrodynamical simulations, thus guaranteeing that the source of feedback in our simulations is a realistic galaxy population. This is the first time such an approach has been adopted and is complementary to existing theoretical studies of galaxy groups and clusters based on self-consistent hydrodynamical simulations.

The main result to emerge from our work is that a large energy input from AGNs (on average, 35% of the available rest mass energy $\epsilon_r M_{BH} c^2$) is required over the entire formation history of haloes in order to reproduce the observed L_X–T relation and halo gas fractions. This supports the conclusion of Bower et al. (2008) derived using purely semianalytic reasoning.

We initially applied our method in a small $L = 62.5\ h^{-1}$ Mpc volume to explore how the bulk properties of groups and poor clusters are affected by different feedback components, concentrating on the L_X–T relation. The noteworthy results of this preliminary investigation are the following

1. The star formation and supernova feedback scheme employed in the Munich L-Galaxies SAM has a negligible effect on the entropy of the ICM, leading to an L_X–T relation that resembles the relation from a simulation with gravitational heating only. By contrast, the mean relation obtained from hydrodynamical simulations with radiative cooling and stellar feedback typically lies closer to the observed one, particularly on cluster scales. However, these simulations tend to overproduce stars, whereas the fraction of baryons locked up in stars within the virial radius of our clusters is, on average, approximately 9%, in excellent agreement wth observational estimates.
2. Incorporating a simple model for quasar mode AGN feedback in a simulation with L-Galaxies stellar feedback leads to X-ray luminosities considerably in excess of observed values, if the thermal coupling efficiency is $\epsilon_f = 0.05$. The choice $\epsilon_f = 0.05$ ensures the local black hole–bulge mass relation is recovered in hydrodynamical simulations including models for black hole growth and associated quasar activity (Di Matteo et al. 2005). However, our results suggest that simulations which employ the quasar mode feedback scheme of Di Matteo et al. (2008) would be unable to explain the observed scaling of X-ray luminosity with temperature.

   We find that reproducing the desired steepening of the L_X–T relation on group scales actually requires a much larger coupling efficiency: $\epsilon_f = 0.4$. In this case, the hot gas fractions of our simulated clusters also broadly agree with observations. This indicates that the balance between quasar and radio mode feedback needs to be adjusted in L-Galaxies if the model is to simultaneously account for the observed properties of galaxies and the ICM.
3. We have implemented the recent Bower et al. (2008) AGN feedback model in a hybrid simulation with stellar feedback from L-Galaxies. In this model, radio mode feedback can eject X-ray emitting gas from central regions of a halo, reducing the gas density and thus X-ray luminosity. This feedback mechanism is more efficient in lower-mass systems, causing the L_X–T relation to become steeper on group scales as desired. Indeed, we find that the relation obtained from our simulation agrees well with observational data on the mass scales probed. This is also true of the hot gas fractions of our simulated objects, demonstrating that significant AGN heating is a key ingredient in shaping groups and clusters.

Once we had established a model capable of reproducing the observed L_X–T relation and gas fractions of groups and poor clusters, we investigated whether this best-fit model could also explain the properties of richer clusters by performing a hybrid simulation in a larger $L = 125\ h^{-1}$ Mpc volume. Our results can be summarised as follows.

1. The observed L_X–T relation is successfully recovered on all mass scales, apart from the occasional object that has an anomalously high temperature due to a recent injection of energy from the central AGN. The variation in scatter along the relation also compares favorably with observations, although there appears to be a lack of objects at the upper-luminosity edge of the observed L_X–T relation since we do not form CC systems in our non-radiative simulations.
2. The gas fractions of our groups and clusters are in broad agreement with observational data, displaying a similar degree of scatter. We find that AGN feedback significantly lowers the hot gas fraction in groups and poor clusters. This is because low-mass systems have a shallow potential well and AGN heating can efficiently drive X-ray emitting gas from their central regions to their outskirts. By contrast, massive clusters retain a greater fraction of their gas (up to 70% of the cosmic baryon fraction) since they have a much larger binding energy and AGN feedback cannot effectively expel gas from the halo.
3. The radial entropy profiles of our simulated clusters begin to flatten off at $r \approx r_{500}$, departing from the scaling $S \propto r^{1.1}$ observed in cluster outskirts. By contrast, observed entropy profiles typically flatten off at smaller radii $r \approx 0.2 r_{200}$ (e.g., Ponman et al. 2003; Pratt et al. 2006). Consequently, we tend to overestimate the core entropy. The core temperature is also higher than expected from observations of similar mass objects. However, profiles can only be reliably measured for X-ray bright objects, which are probably a biased sample of the population of groups and poor clusters. Our model may provide a reasonable description of X-ray underluminous systems for which is it not possible to extract profiles. Nevertheless, if we are to reproduce the observed profiles of the majority of X-ray bright groups and poor clusters, the core entropy and temperature must be reduced, potentially by including radiative cooling in our simulations.

The work described in this paper represents merely the first stage in the development of our method. Even so, we have obtained several encouraging results with this simple initial model. Following this success, we are currently resimulating a sample of rich clusters ($M_{500} \approx 10^{15}\ h^{-1}\ M_\odot$) extracted from the Millennium volume with our best-fit feedback model. In such massive objects the gas cooling time is longer, so the lack of

radiative cooling in our simulations is less of an issue. Indeed, preliminary results suggest that the density, temperature and entropy profiles we obtain are in better agreement with observed profiles. These results will be presented elsewhere.

Our primary goal in future work is to self-consistently incorporate radiative cooling into our hybrid approach, rather than relying on the simple cooling recipes employed in SAMs. These recipes usually assume that haloes have a spherically symmetric isothermal gas distribution but, in general, neither of these assumptions will hold in hydrodynamical simulations. To circumvent this problem, we intend to fully couple SAMs to radiative simulations, so that the gas distribution in the simulation governs star formation, black hole growth and associated feedback in the SAM. This is a non-trivial task, requiring the simulation and SAM to be run simultaneously. Including gas cooling in our simulations should enable us to produce more realistic ICM profiles in cluster cores, where the cooling time is short, since cooling acts to lower the gas entropy in such regions.

Once our model is fully developed and tested, we shall conduct simulations in the full Millennium volume. The idea is to generate a large sample of rich clusters that are consistent with the high-quality X-ray data available on these scales. An example of an important application of such a sample would be modeling the selection functions of X-ray surveys (e.g., Sahlén et al. 2009). This is essential to exploit the full power of clusters as cosmological probes of the expansion history of the universe.

We thank V. Springel for supplying the merger tree software and G. De Lucia for providing the code for the L-Galaxies semianalytic model. We are also grateful to A. Sanderson and A. Vikhlinin for making their observational data available to us. All simulations were performed using the Virgo Consortium Cosmology Machine at the Institute for Computational Cosmology, Durham. This work was supported by a Science and Technology Facilities Council rolling grant.

REFERENCES

Arnaud, M., & Evrard, A. E. 1999, MNRAS, 305, 631
Balogh, M. L., McCarthy, I. G., Bower, R. G., & Eke, V. R. 2008, MNRAS, 385, 1003
Balogh, M. L., Pearce, F. R., Bower, R. G., & Kay, S. T. 2001, MNRAS, 326, 1228
Begelman, M. C., & Meier, D. L. 1982, ApJ, 253, 873
Benson, A. J., Bower, R. G., Frenk, C. S., Lacey, C. G., Baugh, C. M., & Cole, S. 2003, ApJ, 599, 38
Bialek, J. J., Evrard, A. E., & Mohr, J. J. 2001, ApJ, 555, 597
Bîrzan, L., Rafferty, D. A., McNamara, B. R., Wise, M. W., & Nulsen, P. E. J. 2004, ApJ, 607, 800
Blanton, E. L., Sarazin, C. L., McNamara, B. R., & Wise, M. W. 2001, ApJ, 558, L15
Borgani, S., Finoguenov, A., Kay, S. T., Ponman, T. J., Springel, V., Tozzi, P., & Voit, G. M. 2005, MNRAS, 361, 233
Borgani, S., Governato, F., Wadsley, J., Menci, N., Tozzi, P., Quinn, T., Stadel, J., & Lake, G. 2002, MNRAS, 336, 409
Borgani, S., et al. 2004, MNRAS, 348, 1078
Borgani, S., et al. 2006, MNRAS, 367, 1641
Bower, R. G., Benson, A. J., Malbon, R., Helly, J. C., Frenk, C. S., Baugh, C. M., Cole, S., & Lacey, C. G. 2006, MNRAS, 370, 645
Bower, R. G., McCarthy, I. G., & Benson, A. J. 2008, MNRAS, 390, 1399
Brighenti, F., & Mathews, W. G. 2001, ApJ, 553, 103
Brüggen, M. 2003, ApJ, 592, 839
Brüggen, M., Kaiser, C. R., Churazov, E., & Enßlin, T. A. 2002, MNRAS, 331, 545
Bryan, G. L. 2000, ApJ, 544, L1
Cattaneo, A., Dekel, A., Devriendt, J., Guiderdoni, B., & Blaizot, J. 2006, MNRAS, 370, 1651
Cavagnolo, K. W., Donahue, M., Voit, G. M., & Sun, M. 2009, ApJS, 182, 12
Cavaliere, A., Lapi, A., & Menci, N. 2002, ApJ, 581, L1
Chabrier, G. 2003, PASP, 115, 763
Chartas, G., Brandt, W. N., & Gallagher, S. C. 2003, ApJ, 595, 85
Churazov, E., Brüggen, M., Kaiser, C. R., Böhringer, H., & Forman, W. 2001, ApJ, 554, 261
Churazov, E., Sazonov, S., Sunyaev, R., Forman, W., Jones, C., & Böhringer, H. 2005, MNRAS, 363, L91
Cole, S., Lacey, C. G., Baugh, C. M., & Frenk, C. S. 2000, MNRAS, 319, 168
Cora, S. A. 2006, MNRAS, 368, 1540
Cora, S. A., Tornatore, L., Tozzi, P., & Dolag, K. 2008, MNRAS, 386, 96
Cox, T. J., Di Matteo, T., Hernquist, L., Hopkins, P. F., Robertson, B., & Springel, V. 2006, ApJ, 643, 692
Crenshaw, D. M., Kraemer, S. B., & George, I. M. 2003, ARA&A, 41, 117
Croton, D. J., et al. 2006, MNRAS, 365, 11
Dalla Vecchia, C., Bower, R. G., Theuns, T., Balogh, M. L., Mazzotta, P., & Frenk, C. S. 2004, MNRAS, 355, 995
Davé, R., Katz, N., & Weinberg, D. H. 2002, ApJ, 579, 23
Davis, M., Efstathiou, G., Frenk, C. S., & White, S. D. M. 1985, ApJ, 292, 371
De Lucia, G., & Blaizot, J. 2007, MNRAS, 375, 2
De Lucia, G., Kauffmann, G., & White, S. D. M. 2004, MNRAS, 349, 1101
Di Matteo, T., Colberg, J., Springel, V., Hernquist, L., & Sijacki, D. 2008, ApJ, 676, 33
Di Matteo, T., Springel, V., & Hernquist, L. 2005, Nature, 433, 604
Dunkley, J., et al. 2009, ApJS, 180, 306
Esin, A. A., McClintock, J. E., & Narayan, R. 1997, ApJ, 489, 865
Ettori, S., De Grandi, S., & Molendi, S. 2002, A&A, 391, 841
Ettori, S., Dolag, K., Borgani, S., & Murante, G. 2006, MNRAS, 365, 1021
Fabian, A. C., Sanders, J. S., Taylor, G. B., Allen, S. W., Crawford, C. S., Johnstone, R. M., & Iwasawa, K. 2006, MNRAS, 366, 417
Fender, R., et al. 1999, ApJ, 519, L165
Finoguenov, A., Jones, C., Böhringer, H., & Ponman, T. J. 2002, ApJ, 578, 74
Font, A. S., et al. 2008, MNRAS, 389, 1619
Gallo, E., Fender, R. P., & Pooley, G. G. 2003, MNRAS, 344, 60
Granato, G. L., De Zotti, G., Silva, L., Bressan, A., & Danese, L. 2004, ApJ, 600, 580
Hawley, J. F., & Krolik, J. H. 2006, ApJ, 641, 103
Helsdon, S. F., & Ponman, T. J. 2000, MNRAS, 315, 356
Hirose, S., Krolik, J. H., De Villiers, J.-P., & Hawley, J. F. 2004, ApJ, 606, 1083
Horner, D. J. 2001, PhD thesis, Univ. Maryland
Kaiser, N. 1986, MNRAS, 222, 323
Kauffmann, G., Colberg, J. M., Diaferio, A., & White, S. D. M. 1999, MNRAS, 303, 188
Kauffmann, G., & Haehnelt, M. 2000, MNRAS, 311, 576
Kay, S. T. 2004, MNRAS, 347, L13
Kay, S. T., da Silva, A. C., Aghanim, N., Blanchard, A., Liddle, A. R., Puget, J.-L., Sadat, R., & Thomas, P. A. 2007, MNRAS, 377, 317
Kay, S. T., Thomas, P. A., Jenkins, A., & Pearce, F. R. 2004, MNRAS, 355, 1091
Kennicutt, Jr., R. C. 1989, ApJ, 344, 685
Kravtsov, A. V., Nagai, D., & Vikhlinin, A. A. 2005, ApJ, 625, 588
Lemson, G. 2006, arXiv:astro-ph/0608019
Lewis, G. F., Babul, A., Katz, N., Quinn, T., Hernquist, L., & Weinberg, D. H. 2000, ApJ, 536, 623
Lin, Y.-T., Mohr, J. J., & Stanford, S. A. 2003, ApJ, 591, 749
Lloyd-Davies, E. J., Ponman, T. J., & Cannon, D. B. 2000, MNRAS, 315, 689
Mannucci, F., Della Valle, M., Panagia, N., Cappellaro, E., Cresci, G., Maiolino, R., Petrosian, A., & Turatto, M. 2005, A&AS, 433, 807
Markevitch, M. 1998, ApJ, 504, 27
Martin, C. L. 1999, ApJ, 513, 156
McKinney, J. C., & Gammie, C. F. 2004, ApJ, 611, 977
McNamara, B. R., & Nulsen, P. E. J. 2007, ARA&A, 45, 117
McNamara, B. R., Nulsen, P. E. J., Wise, M. W., Rafferty, D. A., Carilli, C., Sarazin, C. L., & Blanton, E. L. 2005, Nature, 433, 45
Meier, D. L. 2001, ApJ, 548, L9
Menci, N., Fontana, A., Giallongo, E., Grazian, A., & Salimbeni, S. 2006, ApJ, 647, 753
Monaco, P., Fontanot, F., & Taffoni, G. 2007, MNRAS, 375, 1189
Muanwong, O., Thomas, P. A., Kay, S. T., & Pearce, F. R. 2002, MNRAS, 336, 527
Muanwong, O., Thomas, P. A., Kay, S. T., Pearce, F. R., & Couchman, H. M. P. 2001, ApJ, 552, L27
Mulchaey, J. S., Davis, D. S., Mushotzky, R. F., & Burstein, D. 2003, ApJS, 145, 39
Nagai, D., Kravtsov, A. V., & Vikhlinin, A. 2007, ApJ, 668, 1

Osmond, J. P. F., & Ponman, T. J. 2004, MNRAS, 350, 1511
Pearce, F. R., Thomas, P. A., Couchman, H. M. P., & Edge, A. C. 2000, MNRAS, 317, 1029
Pedrosa, S., Tissera, P. B., & Scannapieco, C. 2009, MNRAS, 395, L57
Ponman, T. J., Cannon, D. B., & Navarro, J. F. 1999, Nature, 397, 135
Ponman, T. J., Sanderson, A. J. R., & Finoguenov, A. 2003, MNRAS, 343, 331
Pounds, K. A., Reeves, J. N., King, A. R., Page, K. L., O'Brien, P. T., & Turner, M. J. L. 2003, MNRAS, 345, 705
Pratt, G. W., Arnaud, M., & Pointecouteau, E. 2006, A&AS, 446, 429
Puchwein, E., Sijacki, D., & Springel, V. 2008, ApJ, 687, L53
Quilis, V., Bower, R. G., & Balogh, M. L. 2001, MNRAS, 328, 1091
Rasmussen, J., Ponman, T. J., Mulchaey, J. S., Miles, T. A., & Raychaudhury, S. 2006, MNRAS, 373, 653
Rees, M. J., Begelman, M. C., Blandford, R. D., & Phinney, E. S. 1982, Nature, 295, 17
Robertson, B., Cox, T. J., Hernquist, L., Franx, M., Hopkins, P. F., Martini, P., & Springel, V. 2006b, ApJ, 641, 21
Robertson, B., Hernquist, L., Cox, T. J., Di Matteo, T., Hopkins, P. F., Martini, P., & Springel, V. 2006a, ApJ, 641, 90
Romano-Diaz, E., Shlosman, I., Heller, C., & Hoffman, Y. 2009, ApJ, 702, 1250
Romeo, A. D., Sommer-Larsen, J., Portinari, L., & Antonuccio-Delogu, V. 2006, MNRAS, 371, 548
Ruszkowski, M., & Begelman, M. C. 2002, ApJ, 581, 223
Sahlén, M., et al. 2009, MNRAS, 397, 577
Sanderson, A. J. R., O'Sullivan, E., & Ponman, T. J. 2009, MNRAS, 395, 764
Sanderson, A. J. R., Ponman, T. J., Finoguenov, A., Lloyd-Davies, E. J., & Markevitch, M. 2003, MNRAS, 340, 989
Saro, A., De Lucia, G., Dolag, K., & Borgani, S. 2008, MNRAS, 391, 565
Seljak, U., & Zaldarriaga, M. 1996, ApJ, 469, 437
Shakura, N. I., & Syunyaev, R. A. 1973, A&AS, 24, 337
Sijacki, D., & Springel, V. 2006, MNRAS, 366, 397
Sijacki, D., Springel, V., di Matteo, T., & Hernquist, L. 2007, MNRAS, 380, 877
Springel, V. 2005, MNRAS, 364, 1105
Springel, V., & Hernquist, L. 2003, MNRAS, 339, 289
Springel, V., Di Matteo, T., & Hernquist, L. 2005a, ApJ, 620, L79
Springel, V., White, S. D. M., Tormen, G., & Kauffmann, G. 2001, MNRAS, 328, 726
Springel, V., et al. 2005b, Nature, 435, 629
Stanek, R., Rudd, D., & Evrard, A. E. 2009, MNRAS, 394, L11
Suginohara, T., & Ostriker, J. P. 1998, ApJ, 507, 16
Sun, M., Voit, G. M., Donahue, M., Jones, C., Forman, W., & Vikhlinin, A. 2009, ApJ, 693, 1142
Thomas, P. A., & Couchman, H. M. P. 1992, MNRAS, 257, 11
Tornatore, L., Borgani, S., Springel, V., Matteucci, F., Menci, N., & Murante, G. 2003, MNRAS, 342, 1025
Tozzi, P., & Norman, C. 2001, ApJ, 546, 63
Valdarnini, R. 2003, MNRAS, 339, 1117
Vikhlinin, A., Kravtsov, A., Forman, W., Jones, C., Markevitch, M., Murray, S. S., & Van Speybroeck, L. 2006, ApJ, 640, 691
Voit, G. M. 2005, Rev. Mod. Phys., 77, 207
Voit, G. M., Bryan, G. L., Balogh, M. L., & Bower, R. G. 2002, ApJ, 576, 601
Wu, X.-P., & Xue, Y.-J. 2002, ApJ, 569, 112
Wu, X.-P., Xue, Y.-J., & Fang, L.-Z. 1999, ApJ, 524, 22
Xue, Y.-J., & Wu, X.-P. 2000, ApJ, 538, 65
Yoshida, N., Stoehr, F., Springel, V., & White, S. D. M. 2002, MNRAS, 335, 762